

PAPER • OPEN ACCESS

Simultaneous elliptically and radially polarized THz from one-color laser-induced plasma filament

To cite this article: Sen Mou *et al* 2021 *New J. Phys.* **23** 063048

View the [article online](#) for updates and enhancements.



PAPER




Simultaneous elliptically and radially polarized THz from one-color laser-induced plasma filament

OPEN ACCESS

RECEIVED
27 January 2021REVISED
12 May 2021ACCEPTED FOR PUBLICATION
21 May 2021PUBLISHED
17 June 2021

Original content from
this work may be used
under the terms of the
[Creative Commons
Attribution 4.0 licence](#).

Any further distribution
of this work must
maintain attribution to
the author(s) and the
title of the work, journal
citation and DOI.

Sen Mou^{1,*} , Annalisa D'Arco¹ , Luca Tomarchio², Marta Di Fabrizio² ,
Alessandro Curcio³, Stefano Lupi^{2,4} and Massimo Petrarca⁵¹ INFN and Physics Department, University of Rome 'La Sapienza', P.le Aldo Moro 2, 00185 Rome, Italy² Physics Department, University of Rome 'La Sapienza', P.le Aldo Moro 5, 00185 Rome, Italy³ SOLARIS, Krakow, Poland⁴ INFN-LNF, Via E. Fermi 40, 00044 Frascati, Italy⁵ INFN and SBAI, Department of Basic and Applied Sciences for Engineering, University of Rome 'La Sapienza', Via Scarpa 16, 00161 Rome, Italy

* Author to whom any correspondence should be addressed.

E-mail: sen.mou@roma1.infn.it**Keywords:** laser-induced plasma filament, elliptically polarized THz, radially polarized THz

Abstract

THz-based technologies and research applications have seen a rapid increment in recent period together with the development of novel radiation sources based both on relativistic electrons and laser techniques. In this framework, laser-induced plasma filament plays an important role in generating intense and broadband THz radiation. Although many attentions have been paid to THz emission from two-color plasma filaments, one-color plasma emission has been scarcely investigated. In particular, the polarization state of one-color THz emission is still controversial due to the limitations of the existing THz detection techniques, which are incapable of simultaneously detecting elliptically and radially polarized THz radiation. In this manuscript, we develop a novel detection method and unambiguously demonstrate for the first time that one-color laser-induced plasma filament simultaneously emits elliptically and radially polarized THz radiation. These polarization states suggest that the generation mechanism results from electric quadrupole, showing a new route for producing more complex polarization states and THz vortex beams.

1. Introduction

Laser filamentation [1] has aroused a great interest, becoming a field of intense research activity, thanks to its multidisciplinary applications [2–6]. In particular, THz emission by laser filamentation is extremely competitive to other generation mechanisms [7, 8]. Within the framework of filaments as secondary radiation sources, the mechanisms behind the emission of THz pulses attract many attentions due to its capability of generating energetic [9] and broadband [10, 11] (corresponding to single-cycle level) THz radiation. These characteristics are of paramount importance for many applications, e.g. remote sensing [12, 13], linear [11] and non-linear spectroscopy [14]. Moreover, owing to the plasma environment, the generation can be scaled upward with increasing pump laser intensity without the limitation determined by the medium breakdown [15] as in the case of THz generation by crystals [16]. Two main methodologies for THz emission by laser filamentation are known in literature: one-color and two-color emission. THz generation in two-color filament is ascribed to four-wave (FW) mixing and/or photocurrent [17–23]. The polarization of THz from two-color filament [24–29] and the effect of laser chirp on the yield of THz [30] radiation have been deeply investigated.

Compared with the intensive investigations on THz from two-color filament, reports on one-color THz emission are much fewer. On the other hand, the generation mechanisms of THz from one-color plasma are still under debate. The proposed ones are: FW mixing [31], ponderomotive charge separation [32], transition-Cherenkov radiation [33], quadrupoles [34, 35] and so on. Enhancement of THz emission from

one-color plasma has been achieved by biasing one-color plasma [36] and applying a double pump-beam [37]. The polarization of THz from one-color plasma [33, 35, 38, 39] is controversial due to the lack of detection methodology capable of simultaneously detecting elliptically and radially polarized THz as stated in reference [39]. Thus, it is desirable to develop a novel detection methodology capable of simultaneously detecting elliptically and radially polarized THz to comprehensively characterize THz from one-color filament, which is the aim of this work.

In this manuscript, we develop a novel detection methodology capable of simultaneously detecting elliptically and radially polarized THz, which is based on electro-optic sampling (EOS) technique [40] and a spatial mask. This methodology allows us to simultaneously detect elliptically and radially polarized THz radiation for the first time, to our knowledge. The characteristics of these polarization states are described and their spatial distribution are discussed. Radially polarized THz radiation [41–44] finds applications in particle acceleration [45], spectroscopy [46] and THz waveguide [47]. Thus, the generation of this polarization state from one-color filament is very valuable for these applications. The results also shed light on the understanding of the THz generation mechanism in one-color plasma filament. Moreover, our experiments open the road for the production of more complex THz states like vector and vortex beams, which are poorly investigated in the THz spectral range.

2. Results and discussion

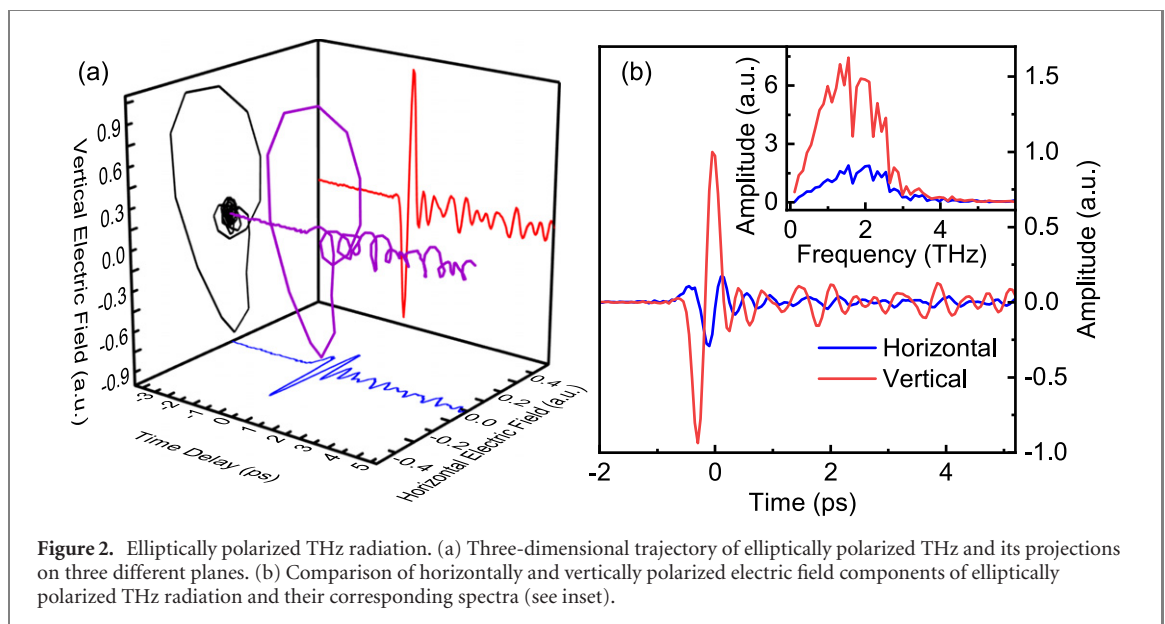
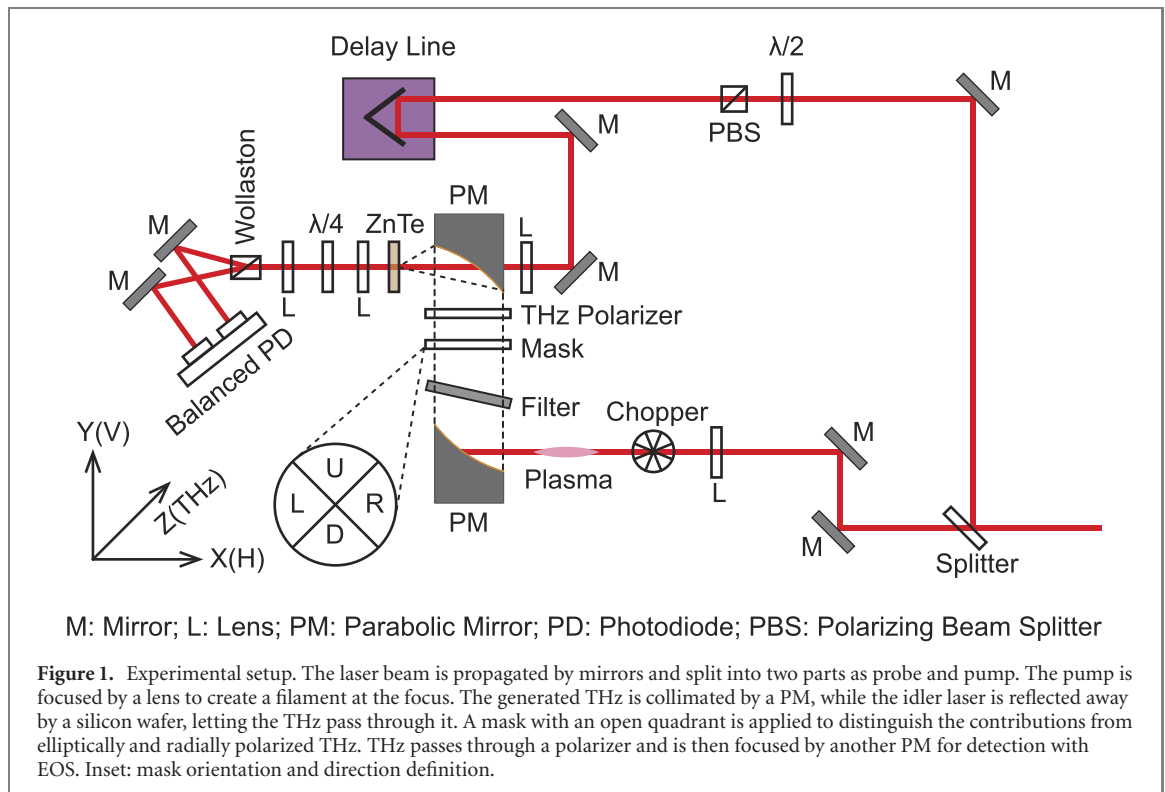
2.1. Experimental setup

The experimental setup is schematically represented in figure 1. The beam, produced by a regenerative amplifier (Coherent Legend) delivering laser pulses with transform-limit duration of $\tau = 50$ fs, central wavelength of $\lambda_0 = 800$ nm and repetition frequency of r.f. = 1 kHz, is split into a pump-line to generate THz and a probe-line to detect THz. The pump pulse is focused by a plano-convex lens with 200 mm focal length to generate the filament. The THz generated from the filament is collimated by an off-axis parabolic mirror (PM) with reflected focal length equal to 6 inches. A silicon wafer is required as a filter to clean the THz from the background radiation (fundamental signal and all the frequencies arising from the non-linear effects appearing during the filamentation process). A metallic mask with an open quadrant is applied onto the THz beam to spatially select a portion of it and then a THz polarizer selects the horizontal or vertical THz electric field component. It is noteworthy that the coincidence of the THz center and the mask center is critical to detect THz in the experiment. Hereby, we use the residual pump as a guide to overlap these centers since the center of THz is the same as that of the pump. To make the center of the residual pump beam overlap the center of the mask, we first center the residual pump beam on an iris and close the iris to its minimum, then we make the mask center coincide with the minimum beam.

Another hole-drilled PM with focal length of 2 inches focuses the THz on a 500 μm -thick 110-cut ZnTe required by the EOS diagnostic module. The intensity of the probe beam can be tuned by a combination of a polarizing beam splitter and a half-wave plate. A delay line is used to change the relative arrival time between the THz and the probe on the ZnTe crystals of the EOS module. A lens focuses the probe through the hole-drilled PM, allowing for the collinear propagation of both the THz and probe beam. It is important to remark that the THz focus spot on the ZnTe crystal is completely covered by the probe-beam one to assure an integrated detection of THz field over its spot size. After the ZnTe crystal, a lens collimates the probe beam through a quarter-wave plate and another lens focuses it again. A Wollaston prism splits the probe into two beams, which are sent to a balanced photodiode. The horizontally polarized pump pulse in the experiment has an energy of 5.7 mJ and FWHM (full width at half maximum) diameter of around 10 mm, creating a single filament with length of around 13 mm. The FWHM diameter of the filament is around 177 μm by measuring its fluorescence. To measure the horizontal and vertical THz field components, the probe polarization is kept horizontal while the $\langle 001 \rangle$ ZnTe crystal axis is varied: it is in the horizontal direction to measure the vertical THz component and it is rotated to the vertical direction to measure the horizontal THz component [40]. Inset of figure 1 shows the mask orientation and the direction definition. The horizontal and vertical field components are in the plane perpendicular to THz propagation axis. The horizontal field component is parallel to the experimental table surface (ZX plane) and the vertical field component is perpendicular to the experimental table surface. The mask can be open up (U), down (D), left (L) and right (R). Generally, in the EOS detection, 110-cut or 100-cut ZnTe (or GaP) crystals are respectively used to measure the transverse or longitudinal components of the field.

2.2. Elliptically polarized THz

We first measure the transverse (horizontal and vertical) electric field components of the THz beam when the spatial mask is not used. In figure 2, the three-dimensional trajectory of the THz field and its projection on the three different planes are shown. The behavior of THz electric field versus time in the



three-dimensional space directly demonstrates that the THz radiation is elliptically polarized. In particular, the red and blue projections in figure 2(a) are respectively the vertical and horizontal polarization components of the elliptically polarized THz beam. These components are directly compared in figure 2(b) in time and in frequency domain (see inset of figure 2(b)), showing that the waveforms of the horizontal and vertical polarization components have different shapes when exhibiting a prominent time shift between them. Moreover, the vertically polarized component is more intense than the horizontal one.

2.3. Radially polarized THz

It is worth noticing that for symmetry reason and in ideal conditions, when an elliptically polarized radiation is focused, it has a zero longitudinal component and a nonzero transverse component at the focus. The opposite happens for radially polarized radiation [48]. Therefore, in order to study the transverse electric field's properties of the emitted THz radiation, we applied a metallic mask on the beam. The mask has a circular shape and it acts as a beam blocker which only transmits through one quadrant over four

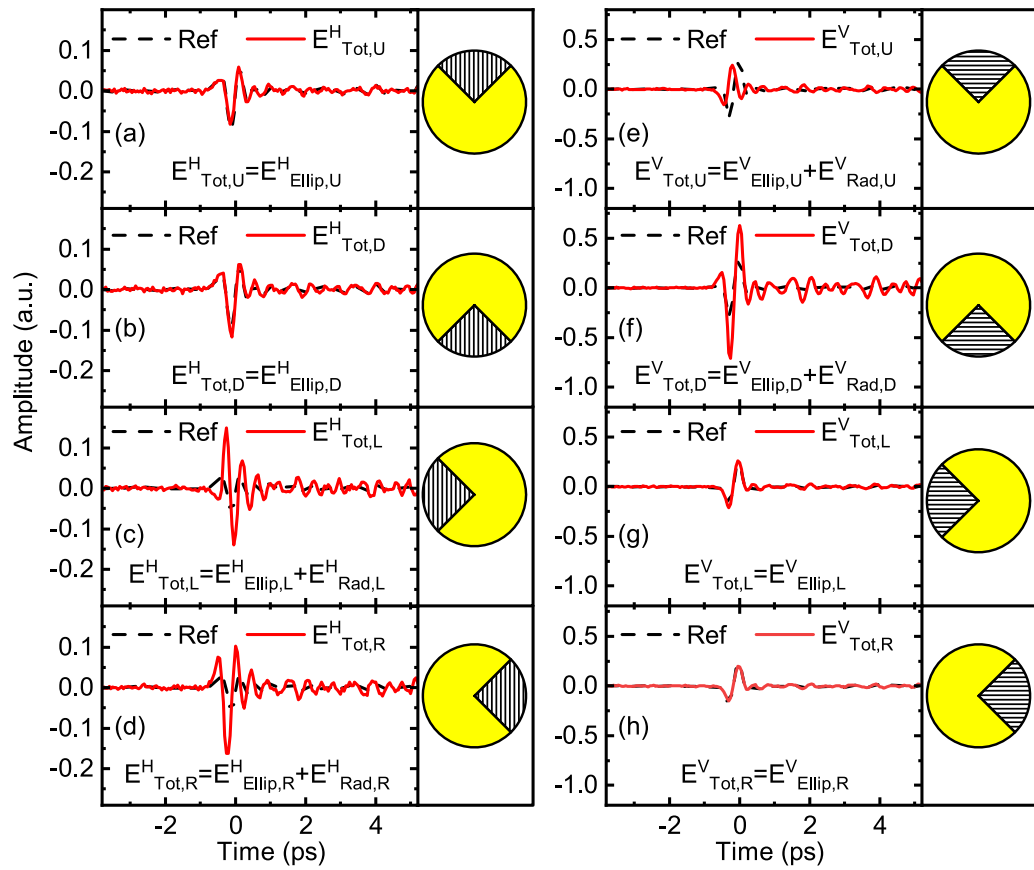


Figure 3. Horizontally and vertically polarized THz in quadrants open in four different directions. Left and right columns respectively show horizontally and vertically polarized THz. (a)–(d) Horizontally polarized THz in quadrants open up and down (left and right). The black dash line is the half sum of THz in quadrants open up and down (left and right). (e)–(h) Similarly for vertically polarized THz in quadrants open up, down, left and right. In (a), (b), (g) and (h), the signal overlaps well with the reference. In (c)–(f), discrepancy between signal and reference is obvious.

(blocking the remaining portions of the beam), see figure 3. We therefore measure both the horizontal and vertical components of the field after the mask and for four different positions of the mask-opening obtained by rotating the mask around the propagation axis of the THz field. The transverse THz field measured in each quadrant is the sum of THz fields originating from both the elliptical and radial THz radiation. Figure 3 shows the result. The combination of the mask-opening and the THz polarizer's direction is shown on the right side of each panel. For the sake of simplicity, we define the following symbol to denote the electric fields measured for the different quadrants:

$$E_{\beta,\gamma}^{\alpha},$$

where $\alpha = \text{H/V}$ indicate respectively the horizontal and vertical polarization components; $\beta = \text{ellip, rad}$ and $\gamma = \text{U, R, D, L}$ respectively denote the polarization state of the electric field (elliptical or radial) and the total field in one quadrant; $\gamma = \text{U, R, D, L}$ shows the mask opening: up, right, down and left. These definitions result in

$$E_{\text{Tot},\gamma}^{\alpha} = E_{\text{Ellip},\gamma}^{\alpha} + E_{\text{Rad},\gamma}^{\alpha}. \quad (1)$$

The THz field is supposed to be symmetric about the horizontal and vertical axes passing through the THz profile center for both the two different states of polarization [35, 49]. Table 1 summarizes the relations between the different field components $E_{\beta,\gamma}^{\alpha}$ due to this symmetry.

In figures 3(a) and (b), the red solid curves represent the total horizontal electric field for the mask opening up and down: $E_{\text{Tot},\text{U}}^{\text{H}}$ and $E_{\text{Tot},\text{D}}^{\text{H}}$. Considering (1) and the relations in table 1, equations of $E_{\text{Tot},\text{U}}^{\text{H}} = E_{\text{Ellip},\text{U}}^{\text{H}}$ and $E_{\text{Tot},\text{D}}^{\text{H}} = E_{\text{Ellip},\text{D}}^{\text{H}}$ hold. The reference black-segmented curves in the same figures show the half sum of the total fields, i.e. $(E_{\text{Tot},\text{U}}^{\text{H}} + E_{\text{Tot},\text{D}}^{\text{H}})/2$. Similarly, in figures 3(c) and (d) the red curves are $E_{\text{Tot},\text{L}}^{\text{H}}$ and $E_{\text{Tot},\text{R}}^{\text{H}}$ with the reference black-segmented curves denoting $(E_{\text{Tot},\text{L}}^{\text{H}} + E_{\text{Tot},\text{R}}^{\text{H}})/2$; in figures 3(e) and (f), the red curves are $E_{\text{Tot},\text{U}}^{\text{V}}$ and $E_{\text{Tot},\text{D}}^{\text{V}}$, and the reference black-segmented curves are $(E_{\text{Tot},\text{U}}^{\text{V}} + E_{\text{Tot},\text{D}}^{\text{V}})/2$. In figures 3(h) and (g), the red curves are $E_{\text{Tot},\text{L}}^{\text{V}}$ and $E_{\text{Tot},\text{R}}^{\text{V}}$ with $E_{\text{Tot},\text{L}}^{\text{V}} = E_{\text{Ellip},\text{L}}^{\text{V}}$ and $E_{\text{Tot},\text{R}}^{\text{V}} = E_{\text{Ellip},\text{R}}^{\text{V}}$, and the reference black-segmented curves are $(E_{\text{Tot},\text{L}}^{\text{V}} + E_{\text{Tot},\text{R}}^{\text{V}})/2$. Equations (2)–(5)

Table 1. Relations between different $E_{\beta,\gamma}^{\alpha}$.

Elliptical THz	Radial THz
$E_{\text{Ellip},R}^H = E_{\text{Ellip},L}^H$	$E_{\text{Rad},R}^H = -E_{\text{Rad},L}^H$
$E_{\text{Ellip},U}^H = E_{\text{Ellip},D}^H$	$E_{\text{Rad},U}^H = E_{\text{Rad},D}^H = 0$
$E_{\text{Ellip},R}^V = E_{\text{Ellip},L}^V$	$E_{\text{Rad},R}^V = E_{\text{Rad},L}^V = 0$
$E_{\text{Ellip},U}^V = E_{\text{Ellip},D}^V$	$E_{\text{Rad},U}^V = -E_{\text{Rad},D}^V$

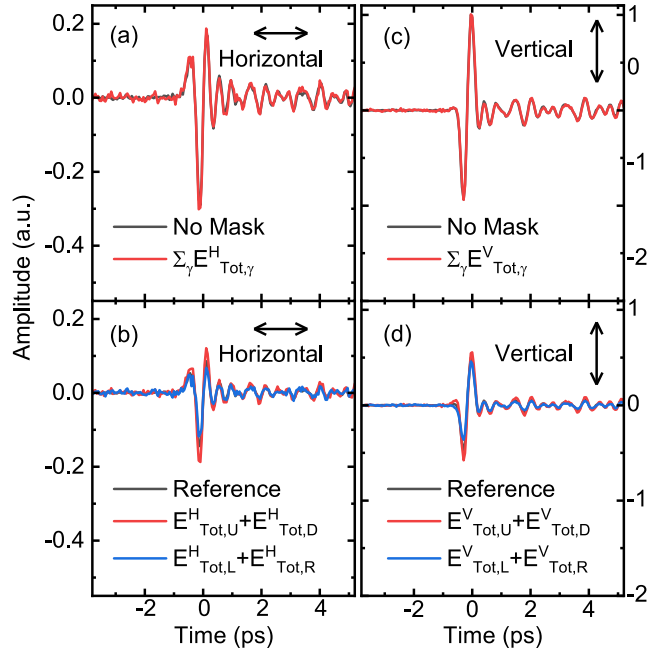


Figure 4. Comparison of elliptically polarized THz measured with and without mask. (a) and (c) Comparison of horizontal (vertical) THz components measured without mask and the sum of horizontal (vertical) fields obtained from the all four different mask-opening directions. The result without mask overlaps well with the sum with mask. (b) and (d) Comparison of the sum of the horizontal (vertical) THz components in the quadrants open up and down vs the quadrants open left and right.

respectively explicitly describe the reference black-segmented curves in figures 3(a)–(h).

$$\frac{E_{\text{Tot},U}^H + E_{\text{Tot},D}^H}{2} = \frac{E_{\text{Ellip},U}^H + E_{\text{Ellip},D}^H}{2} \quad (2)$$

$$\frac{E_{\text{Tot},L}^H + E_{\text{Tot},R}^H}{2} = \frac{E_{\text{Ellip},L}^H + E_{\text{Ellip},R}^H}{2} \quad (3)$$

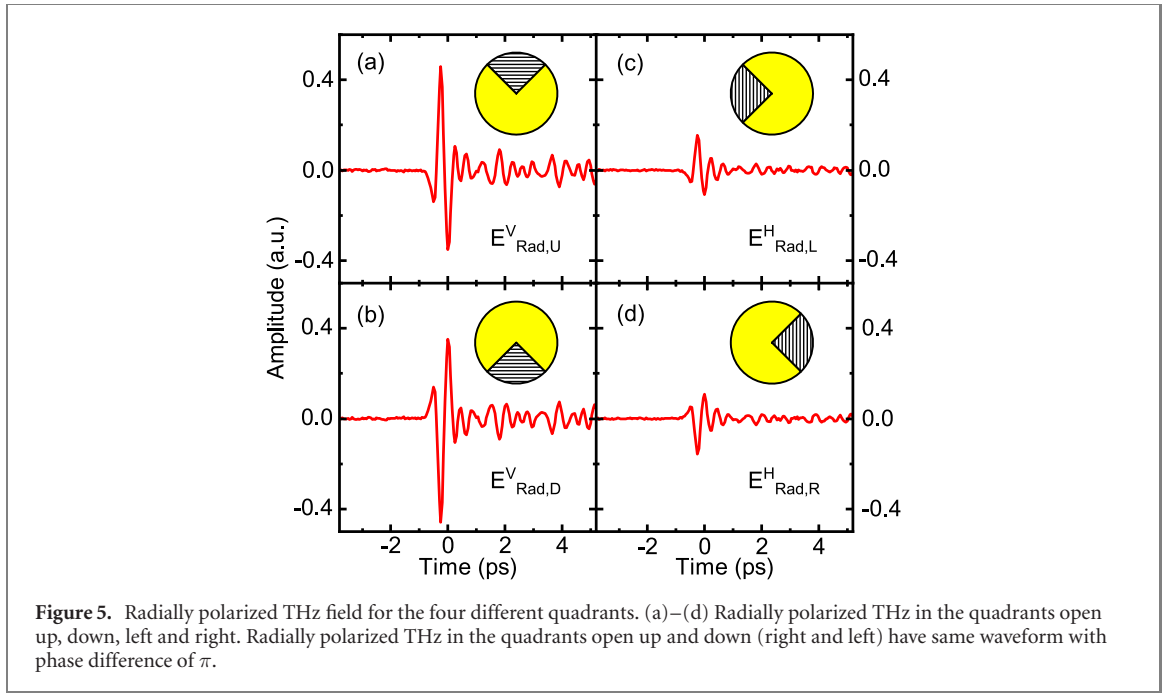
$$\frac{E_{\text{Tot},U}^V + E_{\text{Tot},D}^V}{2} = \frac{E_{\text{Ellip},U}^V + E_{\text{Ellip},D}^V}{2} \quad (4)$$

$$\frac{E_{\text{Tot},L}^V + E_{\text{Tot},R}^V}{2} = \frac{E_{\text{Ellip},L}^V + E_{\text{Ellip},R}^V}{2} \quad (5)$$

Equations (2)–(5) show that the reference curves in figure 3 are only determined by the elliptically polarized THz radiation.

Figures 3(a) and (b) shows a good overlap between the reference and the red curves, i.e. they show that: $E_{\text{Tot},U}^H = E_{\text{Tot},D}^H = (E_{\text{Tot},U}^H + E_{\text{Tot},D}^H)/2$, confirming therefore the third row of table 1. Similarly, the red curves in figures 3(g) and (h) superpose the reference curves very well, justifying the fourth row in table 1. In stark contrast, figures 3(c) and (d) as well as figures 3(e) and (f) demonstrate obvious discrepancies between the reference and the red curves. At this point it is important to anticipate what is experimentally confirmed and shown in figure 4, and which can be deduced from symmetry reasoning: the elliptically polarized THz is the only origin of the reference curves. Thus, the discrepancies observed in figures 3(c)–(f) can only be ascribed to the contribution of the radially polarized THz to the total field represented by the red curves.

In summary, the reference curves in figure 3 are only related to contribution of the elliptical polarization state of the THz radiation, whereas the red curves result from the contributions of both the elliptical and radial polarization states. The good overlaps shown in figures 3(a), (b), (g) and (h) reveal that $E_{\text{Rad},U}^H, E_{\text{Rad},D}^H,$



$E_{\text{Rad,L}}^V$ and $E_{\text{Rad,R}}^V$ are equal to zero. On the contrary, the discrepancies observed in figures 3(c)–(f) manifest a significant contribution of the radial polarization state: $E_{\text{Rad,L}}^H$, $E_{\text{Rad,R}}^H$, $E_{\text{Rad,U}}^V$ and $E_{\text{Rad,D}}^V$.

Equations (2) and (3) demonstrate that both the sum of horizontal THz fields in the upper and lower quadrants ($E_{\text{Tot,U}}^H + E_{\text{Tot,D}}^H$) and the sum in the left and right quadrants ($E_{\text{Tot,L}}^H + E_{\text{Tot,R}}^H$) only result from the elliptically polarized THz radiation. Thus, the sum of horizontal THz fields in the upper and lower quadrants and the sum in the left and right quadrants should have similar waveforms. Furthermore, the sum of horizontal THz fields in all the four quadrants ($\sum_{\gamma} E_{\text{Tot},\gamma}^H$) should be equal to the horizontal THz field detected without mask. Figures 4(a) and (b) clearly verify these two deductions. In fact, figure 4(a) demonstrates that the THz waveform for the sum of the horizontal THz components in the four quadrants overlaps well with that obtained without mask. Meanwhile, figure 4(b) shows that both the waveforms for $E_{\text{Tot,U}}^H + E_{\text{Tot,D}}^H$ and $E_{\text{Tot,L}}^H + E_{\text{Tot,R}}^H$ are similar to the half horizontal field detected without mask, which is the black curve in figure 4(b). The only differences are their amplitudes. Thus, figure 4(b) justifies $E_{\text{Rad,R}}^H = -E_{\text{Rad,L}}^H$ in the second column and second row of table 1.

Similar conclusions can be also drawn for the vertical component of the THz field. The sum of the vertical components in the four quadrants ($\sum_{\gamma} E_{\text{Tot},\gamma}^V$) should be equal to the vertical field measured without mask according to (4) and (5). The waveforms of vertical components in the upper and lower quadrants ($E_{\text{Tot,U}}^V + E_{\text{Tot,D}}^V$) and the sum of vertical fields in the left and right quadrants ($E_{\text{Tot,L}}^V + E_{\text{Tot,R}}^V$) should be similar to the vertical field obtained without mask. Figures 4(c) and (d) confirm these conclusions. Actually, figure 4(c) shows good overlap between the sum of the vertical THz fields in the four quadrants and vertical THz field measured without mask. The reference curve in figure 4(d) is half of the vertical THz field measured without mask. Figure 4(d) demonstrates that the waveforms for $E_{\text{Tot,U}}^V + E_{\text{Tot,D}}^V$ and $E_{\text{Tot,L}}^V + E_{\text{Tot,R}}^V$ match the reference curve except for a small amplitude difference, supporting therefore $E_{\text{Rad,U}}^V = -E_{\text{Rad,D}}^V$ in the last row of table 1.

Moreover, the fact that blue and red curves have the same waveform shape as the reference curve in figures 4(b) and (d) experimentally verifies that the elliptically polarized THz field is the only origin of the reference curves in figure 3. Another characteristic of figures 4(b) and (d) is that the sums of both the horizontal and vertical THz fields in the upper and lower quadrants are bigger than their counterparts in the left and right quadrants. This amplitude difference is addressed to a non-homogeneous spatial distribution of the THz radiation.

Exploiting the characteristics of $E_{\beta,\gamma}^{\alpha}$ shown in table 1, the components $E_{\text{Rad},\gamma}^{\alpha}$ can be extracted by comparing the red and the reference curves shown in figure 3. Due to the symmetry, $E_{\text{Rad,U}}^H$, $E_{\text{Rad,D}}^H$, $E_{\text{Rad,L}}^V$ and $E_{\text{Rad,R}}^V$ are equal to zero. The other four components $E_{\text{Rad},\gamma}^{\alpha}$ are obtained by subtracting the reference from the red curves in figures 3(c)–(f). $E_{\text{Rad,U}}^V$, $E_{\text{Rad,D}}^V$, $E_{\text{Rad,L}}^H$ and $E_{\text{Rad,R}}^H$ are shown in figure 5, which shows that $E_{\text{Rad,U}}^V$ and $E_{\text{Rad,L}}^H$ ($E_{\text{Rad,D}}^H$ and $E_{\text{Rad,R}}^V$) are in phase and have the same waveform shape but with different amplitudes. Whereas, $E_{\text{Rad,U}}^V$ and $E_{\text{Rad,D}}^V$ ($E_{\text{Rad,L}}^H$ and $E_{\text{Rad,R}}^H$) have the same waveform but phase shift of π as expected by the natural characteristics of radial polarization state.

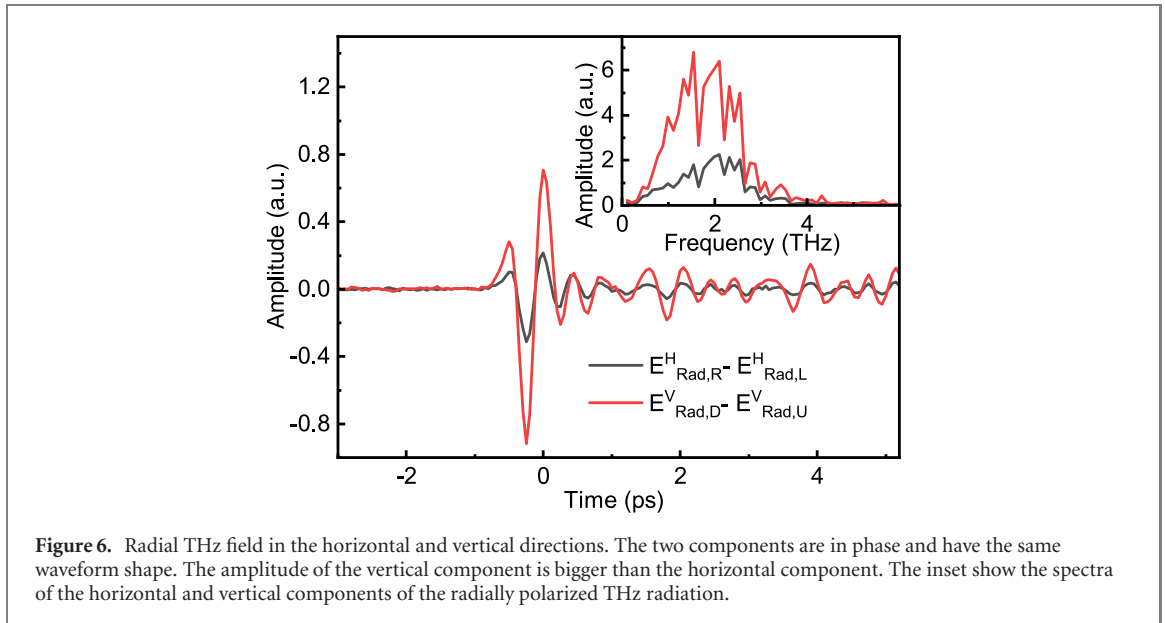


Figure 6. Radial THz field in the horizontal and vertical directions. The two components are in phase and have the same waveform shape. The amplitude of the vertical component is bigger than the horizontal component. The inset show the spectra of the horizontal and vertical components of the radially polarized THz radiation.

From table 1, the subtraction of the red curve in figures 3(c) and (e) from the red curve in figures 3(d) and (f) results in $E_{\text{Rad,D}}^{\text{V}} - E_{\text{Rad,U}}^{\text{V}}$ ($E_{\text{Rad,R}}^{\text{H}} - E_{\text{Rad,L}}^{\text{H}}$). We use $E_{\text{Rad,D}}^{\text{V}} - E_{\text{Rad,U}}^{\text{V}}$ and $E_{\text{Rad,R}}^{\text{H}} - E_{\text{Rad,L}}^{\text{H}}$ to respectively stand for radial THz in the vertical and horizontal directions. The main panel of figure 6 shows these results in time domain while the inset in the frequency domain. It can be seen that the waveforms of radial THz in the horizontal and vertical directions are in phase and have the same waveform but with different amplitudes. Moreover, the amplitude of the radial THz in vertical direction is stronger than that in the horizontal direction, which is consistent with the reported quadrupole-type THz radiation pattern [49, 50], suggesting that THz from one-color filament may result from quadrupole. The different intensities of the radially polarized THz in the horizontal and vertical directions are determined by the polarization of the pump laser. In order to check the relation between the pump polarization and the intensities of the radially polarized THz in the horizontal and vertical directions, we measured the intensities of the radially polarized THz in the horizontal and vertical directions as a function of the pump polarization. It was found that the strongest intensity of the radially polarized THz in the horizontal direction appears near to the vertical pump polarization. Whereas, the strongest in the vertical direction appears near to the horizontal pump polarization. It is noteworthy that the radial THz in the horizontal and vertical directions are in phase and have the same waveform shape, whereas the horizontal and vertical THz fields of elliptically polarized THz are out of phase and have different waveform shapes as shown in figure 2(b).

3. Conclusion

In this manuscript, we demonstrate that one-color laser-induced filament simultaneously radiates elliptically and radially polarized THz radiation. We measured the horizontal and vertical components of the elliptically polarized field and extracted the fields of the radially polarized THz radiation through a metallic opaque mask. The results of this paper shade light on THz generation mechanism from one-color filament, indicating that the main generation mechanism is related to quadrupole formation, and suggest that more complex vortex THz beams could be realized in plasma starting from structured pump-laser. The radially polarized (and vortex) THz radiation can be used in spectroscopic applications on exotic quantum matter.

Acknowledgments

The authors acknowledge the TERA INFN project for supporting this research.

Data availability statement

All data that support the findings of this study are included within the article (and any supplementary files).

ORCID iDs

Sen Mou  <https://orcid.org/0000-0002-6872-9389>

Annalisa D'Arco  <https://orcid.org/0000-0001-7990-5117>

Marta Di Fabrizio  <https://orcid.org/0000-0003-3812-5995>

References

- [1] Couairon A and Mysyrowicz A 2007 Femtosecond filamentation in transparent media *Phys. Rep.* **441** 47–189
- [2] Petrarca M, Petit Y, Henin S, Delagrange R, B ejot P and Kasparian J 2012 Higher-order kerr improve quantitative modeling of laser filamentation *Opt. Lett.* **37** 4347–9
- [3] Liu X-L, Cheng W, Petrarca M and Polynkin P 2016 Measurements of fluence profiles in femtosecond laser filaments in air *Opt. Lett.* **41** 4751–4
- [4] Petrarca M et al 2014 White-light femtosecond Lidar at 100 TW power level *Appl. Phys. B* **114** 319–25
- [5] Saathoff H et al 2013 Laser filament-induced aerosol formation *Atmos. Chem. Phys.* **13** 4593–604
- [6] Kartashov D et al 2013 Mid-infrared laser filamentation in molecular gases *Opt. Lett.* **38** 3194–7
- [7] Chiadroni E et al 2013 The SPARC linear accelerator based terahertz source *Appl. Phys. Lett.* **102** 094101
- [8] Perucchi A, Di Mitri S, Penco G, Allaria E and Lupi S 2013 The terafermi terahertz source at the seeded fermi free-electron-laser facility *Rev. Sci. Instrum.* **84** 022702
- [9] Kuk D, Yoo Y J, Rosenthal E W, Jhajj N, Milchberg H M and Kim K Y 2016 Generation of scalable terahertz radiation from cylindrically focused two-color laser pulses in air *Appl. Phys. Lett.* **108** 121106
- [10] Matsubara E, Nagai M and Ashida M 2012 Ultrabroadband coherent electric field from far infrared to 200 THz using air plasma induced by 10 fs pulses *Appl. Phys. Lett.* **101** 011105
- [11] Mou S, Rubano A and Paparo D 2018 Broadband terahertz spectroscopy of imidazolium-based ionic liquids *J. Phys. Chem. B* **122** 3133–40
- [12] Liu J, Dai J, Chin S L and Zhang X-C 2010 Broadband terahertz wave remote sensing using coherent manipulation of fluorescence from asymmetrically ionized gases *Nat. Photon.* **4** 627–31
- [13] Stelmaszczyk K, Rohwetter P, M ejjean G, Yu J, Salmon E, Kasparian J, Ackermann R, Wolf J-P and W oste L 2004 Long-distance remote laser-induced breakdown spectroscopy using filamentation in air *Appl. Phys. Lett.* **85** 3977–9
- [14] Giorgianni F et al 2016 Strong nonlinear terahertz response induced by Dirac surface states in Bi₂Se₃ topological insulator *Nat. Commun.* **7** 11421
- [15] Curcio A and Petrarca M 2020 Saturation regime of THz generation in nonlinear crystals by pumps with arbitrary spectral modulations *Opt. Lett.* **45** 1619–22
- [16] Oh T I, You Y S, Jhajj N, Rosenthal E W, Milchberg H M and Kim K Y 2013 Intense terahertz generation in two-color laser filamentation: energy scaling with terawatt laser systems *New J. Phys.* **15** 075002
- [17] Cook D J and Hochstrasser R M 2000 Intense terahertz pulses by four-wave rectification in air *Opt. Lett.* **25** 1210–2
- [18] Xie X, Dai J and Zhang X-C 2006 Coherent control of THz wave generation in ambient air *Phys. Rev. Lett.* **96** 075005
- [19] Bartel T, Gaal P, Reimann K, Woerner M and Elsaesser T 2005 Generation of single-cycle THz transients with high electric-field amplitudes *Opt. Lett.* **30** 2805–7
- [20] Houard A, Liu Y, Prade B and Mysyrowicz A 2008 Polarization analysis of terahertz radiation generated by four-wave mixing in air *Opt. Lett.* **33** 1195–7
- [21] Kim K-Y, Glowacki J H, Taylor A J and Rodriguez G 2007 Terahertz emission from ultrafast ionizing air in symmetry-broken laser fields *Opt. Express* **15** 4577–84
- [22] Andreeva V A et al 2016 Ultrabroad terahertz spectrum generation from an air-based filament plasma *Phys. Rev. Lett.* **116** 063902
- [23] Kress M, L offler T, Eden S, Thomson M and Roskos H G 2004 Terahertz-pulse generation by photoionization of air with laser pulses composed of both fundamental and second-harmonic waves *Opt. Lett.* **29** 1120–2
- [24] Zhang Z et al 2018 Manipulation of polarizations for broadband terahertz waves emitted from laser plasma filaments *Nat. Photon.* **12** 554–9
- [25] Dai J, Karpowicz N and Zhang X-C 2009 Coherent polarization control of terahertz waves generated from two-color laser-induced gas plasma *Phys. Rev. Lett.* **103** 023001
- [26] Wen H and Lindenberg A M 2009 Coherent terahertz polarization control through manipulation of electron trajectories *Phys. Rev. Lett.* **103** 023902
- [27] Zhang Z, Chen Y, Chen M, Zhang Z, Yu J, Sheng Z and Zhang J 2016 Controllable terahertz radiation from a linear-dipole array formed by a two-color laser filament in air *Phys. Rev. Lett.* **117** 243901
- [28] You Y S, Il Oh T and Kim K-Y 2013 Mechanism of elliptically polarized terahertz generation in two-color laser filamentation *Opt. Lett.* **38** 1034–6
- [29] Kosareva O et al 2018 Polarization control of terahertz radiation from two-color femtosecond gas breakdown plasma *Opt. Lett.* **43** 90–3
- [30] Zhang Z et al 2018 Optimum chirp for efficient terahertz generation from two-color femtosecond pulses in air *Appl. Phys. Lett.* **113** 241103
- [31] Zhang Y et al 2008 Non-radially polarized THz pulse emitted from femtosecond laser filament in air *Opt. Express* **16** 15483–8
- [32] Hamster H, Sullivan A, Gordon S and Falcone R W 1994 Short-pulse terahertz radiation from high-intensity-laser-produced plasmas *Phys. Rev. E* **49** 671–7
- [33] D'Amico C, Houard A, Franco M, Prade B, Mysyrowicz A, Couairon A and Tikhonchuk V T 2007 Conical forward THz emission from femtosecond-laser-beam filamentation in air *Phys. Rev. Lett.* **98** 235002
- [34] Jahangiri F, Hashida M, Nagashima T, Tokita S, Hangyo M and Sakabe S 2011 Intense terahertz emission from atomic cluster plasma produced by intense femtosecond laser pulses *Appl. Phys. Lett.* **99** 261503
- [35] Jahangiri F, Hashida M, Tokita S, Nagashima T, Hangyo M and Sakabe S 2013 Enhancing the energy of terahertz radiation from plasma produced by intense femtosecond laser pulses *Appl. Phys. Lett.* **102** 191106
- [36] Houard A, Liu Y, Prade B, Tikhonchuk V T and Mysyrowicz A 2008 Strong enhancement of terahertz radiation from laser filaments in air by a static electric field *Phys. Rev. Lett.* **100** 255006

- [37] Liu Y, Houard A, Prade B, Akturk S, Mysyrowicz A and Tikhonchuk V T 2007 Terahertz radiation source in air based on bifilamentation of femtosecond laser pulses *Phys. Rev. Lett.* **99** 135002
- [38] Zhao J, Gao H, Li S, Liu C, Chen Y, Peng Y and Zhu Y 2018 Investigating the non-radially polarized component of terahertz wave emission during single-colour femtosecond laser filamentation in air *J. Opt.* **20** 105502
- [39] Chen Y, Marceau C, Liu W, Sun Z-D, Zhang Y, Théberge F, Châteauneuf M, Dubois J and Chin S L 2008 Elliptically polarized terahertz emission in the forward direction of a femtosecond laser filament in air *Appl. Phys. Lett.* **93** 231116
- [40] Planken P C M, Nienhuys H-K, Bakker H J and Wenckebach T 2001 Measurement and calculation of the orientation dependence of terahertz pulse detection in ZnTe *J. Opt. Soc. Am. B* **18** 313–7
- [41] Winnerl S, Zimmermann B, Peter F, Schneider H and Helm M 2009 Terahertz Bessel–Gauss beams of radial and azimuthal polarization from microstructured photoconductive antennas *Opt. Express* **17** 1571–6
- [42] Winnerl S, Hubrich R, Mittendorff M, Schneider H and Helm M 2012 Universal phase relation between longitudinal and transverse fields observed in focused terahertz beams *New J. Phys.* **14** 103049
- [43] Woldegeorgis A, Kurihara T, Almassarani M, Beleites B, Grosse R, Ronneberger F and Gopal A 2018 Multi-mv/cm longitudinally polarized terahertz pulses from laser-thin foil interaction *Optica* **5** 1474–7
- [44] Imai R, Kanda N, Higuchi T, Zheng Z, Konishi K and Kuwata-Gonokami M 2012 Terahertz vector beam generation using segmented nonlinear optical crystals with threefold rotational symmetry *Opt. Express* **20** 21896–904
- [45] Nanni E A, Huang W R, Hong K-H, Ravi K, Fallahi A, Moriena G, Dwayne Miller R J and Kärtner F X 2015 Terahertz-driven linear electron acceleration *Nat. Commun.* **6** 8486
- [46] Sirenko A A, Marsik P, Bernhard C, Stanislavchuk T N, Kiryukhin V and Cheong S-W 2019 Terahertz vortex beam as a spectroscopic probe of magnetic excitations *Phys. Rev. Lett.* **122** 237401
- [47] Deibel J A, Wang K, Escarra M D and Mittleman D 2006 Enhanced coupling of terahertz radiation to cylindrical wire waveguides *Opt. Express* **14** 279–90
- [48] Minami Y, Kurihara T, Yamaguchi K, Nakajima M and Suemoto T 2013 Longitudinal terahertz wave generation from an air plasma filament induced by a femtosecond laser *Appl. Phys. Lett.* **102** 151106
- [49] Fadeev D A, Ilyakov I E, Mironov V A, Suvorov E V, Fadeev D A and Shishkin B V 2009 Plasma mechanisms of pulsed terahertz radiation generation *Radiophys. Quantum Electron.* **52** 482
- [50] Zharova N A, Mironov V A and Fadeev D A 2010 Anisotropic effects of terahertz emission from laser sparks in air *Phys. Rev. E* **82** 056409